Distribution and Dynamics of Adamantanes in a Lipid Bilayer

Chee Foong Chew, Andrew Guy, and Philip C. Biggin
Department of Biochemistry, University of Oxford, Oxford OX1 3QU, United Kingdom

ABSTRACT The adamantanes are a class of compounds that have found use in the treatment of influenza A and Parkinson's disease, among others. The mode of action for influenza A is based on the adamantanes' interaction with the transmembrane M2 channel, whereas the treatment of Parkinson's disease is thought to relate to a channel block of *N*-methyl-D-aspartate receptors. An understanding of how these compounds interact with the lipid bilayer is thus of great interest. We used molecular-dynamics simulations to calculate the potential of mean force of adamantanes in a lipid bilayer. Our results demonstrate a preference for the interfacial region of the lipid bilayer for both protonated and deprotonated species, with the protonated species proving significantly more favorable. However, the protonated species have a large free-energy barrier in the center of the membrane. In contrast, there is no barrier (compared with aqueous solution) at the center of the bilayer for deprotonated species, suggesting that the permeant species is indeed the neutral form, as commonly assumed. We discuss the results with respect to proposed mechanisms of action and implications for drug-delivery in general.

INTRODUCTION

Adamantane (tricyclo-decane) derivatives are a series of compounds (Fig. 1) widely used in the treatment of various diseases, including influenza (1) and Parkinson's disease (2). Amantadine (1-aminoadamantane) is perhaps the most widely studied adamantane derivative. It is one of the oldest compounds known to have an antiviral effect against influenza A (1,3–5), and was first approved by the Food and Drug Administration in 1966 (www.fda.gov). Since then, the related compound rimantadine has also been approved. The antiviral action of both compounds is thought to arise from inhibition of the M2 channel, a viroporin of influenza A (5). Amantadine was also suggested to inhibit another viroporin, the p7 protein of hepatitis C virus (HCV) (6). However, more recent work suggested that amantadine had no effect on p7 ion-channel activity or the infectivity of HCV particles (7). Nevertheless, amantadine was used in clinical trials to treat HCV (8). Some of these trials reported success (9–12), but controversy persists about the effectiveness of amantadine in the clinic (13–17).

Amantadine and memantine (18) (Fig. 1) have also been used in the treatment of Parkinson's disease (19–21), with a block of the *N*-methyl-D-aspartic acid (NMDA) receptors as the most likely mode of action (22–24). However, according to other reports, amantadine interacts with nicotinic acetylcholine receptors (23), raising the possibility of neuronal nicotinic acetylcholine receptors as drug targets in the treatment of Parkinson's disease (25). Memantine is also thought to target NMDA receptors in the treatment of Alzheimer's disease (26), and was recently used in the treatment of glaucoma (27).

Amantadine and related compounds were shown to stabilize clathrin-coated vesicles and lipid membranes, suggesting a possible role in inhibition of ligand uptake (28,29). In addition, it was suggested that the therapeutic activity of amantadine is related to nonspecific interactions (28–30).

Thus, adamantane derivatives appear to have many possible roles as therapeutic agents. At the molecular level, though, the action of amantadine against the influenza A M2 channel has received the most attention (1). The single transmembrane domain of each M2 protein consists of an α-helix, and a minimum of four of these is required to make a functional channel that conducts protons. The most obvious mode of action for amantadine is simply to sit inside the helical bundle and thus block the pore (31). Indeed, two mutations that result in resistance to amantadine occur on residues that are thought to line the pore (A30T and G34E) (4). However, this ''cork in the bottle'' mechanism is not easily reconciled with some of the electrophysiological observations (32), or with results obtained from amantadine-resistant mutants (33), and thus the precise mode of action of amantadine remains controversial.

Hu et al. speculated that amantadine action might not involve a simple block, but that interference with the His-37 residues facilitates proton conductance (34). Fluorescence spectroscopy and circular dichroism experiments also suggest a subtle change in the structure of the M2 channel in the presence of amantadine (35). The location of amantadine-resistant mutants suggests that amantadine resides in the external membrane leaflet. Furthermore, amantadine only inhibits channel activity when it is applied to the medium that bathes the N-terminal ectodomain (10 μM is enough), and not when applied to the C-terminal tail (even in the presence of 1 mM) (36). More recently, both an x-ray structure and an NMR structure of M2 in complex with amantadine (37) and rimantadine (38), respectively, were described. Interest-

Submitted June 12, 2008, and accepted for publication September 5, 2008.

Address reprint requests to Philip Biggin, Structural Bioinformatics and Computational Biochemistry, Dept. of Biochemistry, University of Oxford, South Parks Road, Oxford OX1 3QU, UK. Tel.: 44-1865-275255; Fax: 44-1865-275273; E-mail: philip.biggin@bioch.ox.ac.uk.

Editor: Peter C. Jordan.

0006-3495/08/12/5627/10 $2.00

doi: 10.1529/biophysj.108.139477

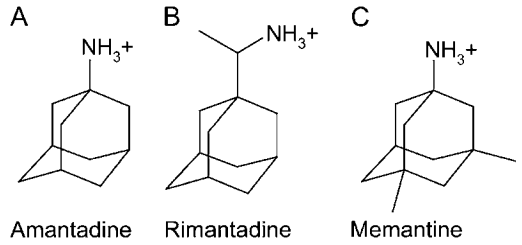

FIGURE 1 Structure of amantadine (*A*), rimantadine (*B*), and memantine (*C*).

ingly, two different modes of interaction were reported. The amantadine structure supported the channel-block hypothesis, whereas the rimantadine structure suggested an interaction with the exterior of the M2 channel. Solid-state NMR experiments implied that amantadine can alter the conformational equilibrium of the M2 channel, and that amantadine-resistant mutations create changes in this equilibrium that result in altered binding properties (39).

Whatever the precise mode of interaction, it seems likely that lipophilic compounds such as amantadine may reach the channel after first partitioning into the membrane. If one additionally considers the role of adamantanes in the treatment of neurodegenerative disorders, then permeation across the membrane becomes an important consideration with respect to the blood-brain barrier and pharmacokinetics (40).

Neutron and x-ray diffraction studies using 1,2-dioleoyl-*sn*-glycero-3-phosphocholine (DOPC) showed that the majority of amantadine interacts with the lipid headgroups close to the surface of membrane, whereas a minor proportion penetrates deeper into the bilayer (41). Recent experiments suggest that amantadine is significantly more soluble in lipid bilayers than in aqueous solution (42,43). The experiments of Subczynski et al. (43) also suggest that amantadine is more soluble in lipid bilayers than in bulk hydrocarbon solvent. These experiments did not indicate the precise location of amantadine in the lipid bilayer, or how amantadine may cross the bilayer. An understanding of this may be particularly timely, given that amantadine leads to undesirable side effects within the central nervous system (44). Furthermore, the issue of amantadine-resistant forms of the influenza A virus is of increasing concern (45–47). During the 2005–2006 influenza season, 92.3% of influenza A virus isolated from patients across the United States contained the amantadine-resistant (S31N) mutation (48). High levels of amantadine-resistant forms were also observed in Southeast Asia and Oceania (49), as well as in Japan (50).

Molecular dynamics (MD) is methodology than can provide detailed atomic-level descriptions of systems, and is thus a complementary method to the above series of experiments. Indeed, there are many examples of MD simulations in the investigation of the interactions of small molecules with lipid membranes (51). One of the first sets of simulations (52–55) examined diffusion coefficient solutes such as benzene in dimyristoylphosphatidylcholine bilayers. Several groups explored the interaction of anesthetic molecules with lipid bilayers (56–59), and Bemporad et al. systematically examined the influence of various solute properties (e.g., volume or cross-sectional area) on lipid-solute interactions (60,61), as well as on interactions of β-blockers with membranes (62).

The potential of mean force (PMF) is free energy as a function of a reaction coordinate. As the PMF profile depends on both enthalpic and entropic contributions, its precise calculation has long been a challenge to MD, because thermodynamically unfavorable regions are not well-sampled (63). One of several methods that were developed for PMF calculations is umbrella sampling, which applies a biasing potential to obtain better sampling in thermodynamically unfavorable regions (64).

The PMFs have provided mechanistic insights about the transport mechanism of ions in channels (65), in particular for the gramicidin ion channel. Beckstein and Sansom calculated PMFs to investigate gating mechanisms of the nicotinic acetylcholine receptor (66). The PMFs were also used to understand the mechanism of lipid desorption (67) and the localization of indole rings in lipid bilayers (68). More recently, the PMF of an arginine side-chain in a bilayer was calculated (69,70), with a view to understanding the mechanism of voltage-sensing in potassium channels.

Here we perform PMF calculations to calculate: 1), the preferred location and orientation of three adamantanes (amantadine, rimantadine, and memantine) in the bilayer; 2), the energetic costs associated with those positions; and 3), the preference for protonation states of these compounds at different locations across the bilayer. Our results support the hypothesis that these compounds absorb into the lipid bilayer and prefer an interfacial location.

METHODS

Each simulation system consists of one adamantine molecule (amantadine, rimantadine, or memantine; Fig. 1), 52 1-palmitoyl-2-oleoyl-*sn*-glycero-3-phosphatidylcholine (POPC) lipids in the initial setup, 1820 simple point charge (SPC) water molecules (71), and one chloride ion. The topology of adamantanes was obtained from the PRODRG (72) server, and charges on atoms were recalculated at the Hartree-Fock 6-31G* level, using Spartan '02 (Wavefunction, Irvine, CA). Charges and atom types in systems are given explicitly in the Supplementary Material (Data S1). The one-dimensional (1D) PMF was calculated using umbrella sampling. The 1D reaction coordinate is along the z axis, which corresponds to the bilayer normal. The umbrella potential acts on the center of mass of amantadine, with an initial harmonic potential of force constant of 2.4 kcal mol^{-1} Å^{-2} (10 kJ mol^{-1} Å^{-2}). We found that this force constant was too weak in the center of the bilayer, and thus we systematically tested force constants up to 1194 kcal mol^{-1} Å^{-2} (5000 kJ mol^{-1} Å^{-2}). The starting configuration for each umbrella window was obtained by placing the adamantine molecule independently at different z coordinates, to include 190 windows each separated by a width $\Delta z = 0.5$ Å. Each window was subjected to 1000 steps of steepest-descents energy minimization to remove bad contacts with lipid molecules, followed by 1 ns of restrained dynamics, whereby the amantadine was held fixed and the rest of the system was free to move. Each window was first simulated for 15 ns, with the first 2 ns considered an equilibration period, because trajectories afterward are statistically uncorrelated and are within an error of ~1 kcal/mol from the block average. Bad

contacts with lipid chains were minimized out with the steepest-descents algorithm. The system size is $47 \times 47 \times 92$ Å. The PMF profile was constructed from the biased distributions of the centers of mass of amantadine, using the weighted-histogram analysis method with 300–500 bins, and a relative tolerance of 10^{-5} for the individual window offset. Statistical tests, described by Schiferl and Wallace (73), were used to assure the convergence of free-energy calculations, and to estimate the errors in free-energy profiles in the following manner. Trajectories were divided into eight blocks of varying time lengths. Blocks were determined to be uncorrelated by application of a Mann-Kendall test ($\tau = 0.12, n = 8$) and a one-tailed von Neumann test ($x = 0.23, n = 8$). The Shapiro-Wilks test was used on blocks of data to determine the normality of the distribution of mean values ($W = 0.7, p < 0.05, n = 8$).

Simulations were performed with GROMACS 3.2.1 (74) at 310 K and a pressure of 1 bar. Additional simulations were performed with the optimized potential for liquid simulation (OPLS) all-atom force field (75–77), to assess the influence of parameter choice (see the Supplementary Material, Data S1). The Berendsen algorithm was used to couple the temperature of the system with a coupling constant of 1 ps (78). The system pressure was coupled in semi-isotropic fashion (x and y, independent of z), using the Berendsen algorithm with a compressibility of 1×10^{-5} bar^{-1} and a coupling constant of 1 ps (78). Lipid force-field parameters were taken from Berger et al. (79). Electrostatic interactions were accounted for by a particle-mesh Ewald method (80) with a real-space cutoff of 10 Å, a grid spacing of 0.015 Å, and fourth-order interpolation. The van der Waals interactions were computed with a cutoff of 10 Å. The time step was 2 fs. Simulations were run on a Linux cluster. Structures and animations were displayed using Visual Molecular Dynamics (81). The analysis was performed using GROMACS and a locally written code.

RESULTS

Construction of potential of mean force

Fig. 2 shows PMFs as a function of the center of mass derived for the adamantanes in both protonated and deprotonated forms. The protonated forms (Fig. 2, *A–C*) exhibit similarly shaped profiles, with a favorable free-energy well of between −4 and −7 kcal/mol centered around 12 Å from the center of the bilayer, corresponding to the interface. The profiles suggest that as the protonated forms approach the center of the bilayer, they experience a large (11–14 kcal/mol) barrier. Whereas the PMFs for protonated amantadine (Fig. 2 *A*) and rimantadine (Fig. 2 *B*) look similar, the PMF for protonated memantine (Fig. 2 *C*) has a lower barrier at the center of the bilayer. The PMF profiles for deprotonated forms show that the barrier is effectively removed, and the interaction is slightly favorable by 0.7–2.7 kcal/mol (with respect to bulk water) in all three adamantanes (Fig. 2, *D–F*). Although the position of the well in the PMFs is preserved, deprotonation reduces the depth of the well for all three compounds, suggesting that charge interactions are important in determining the extent to which the molecules interact with the interface.

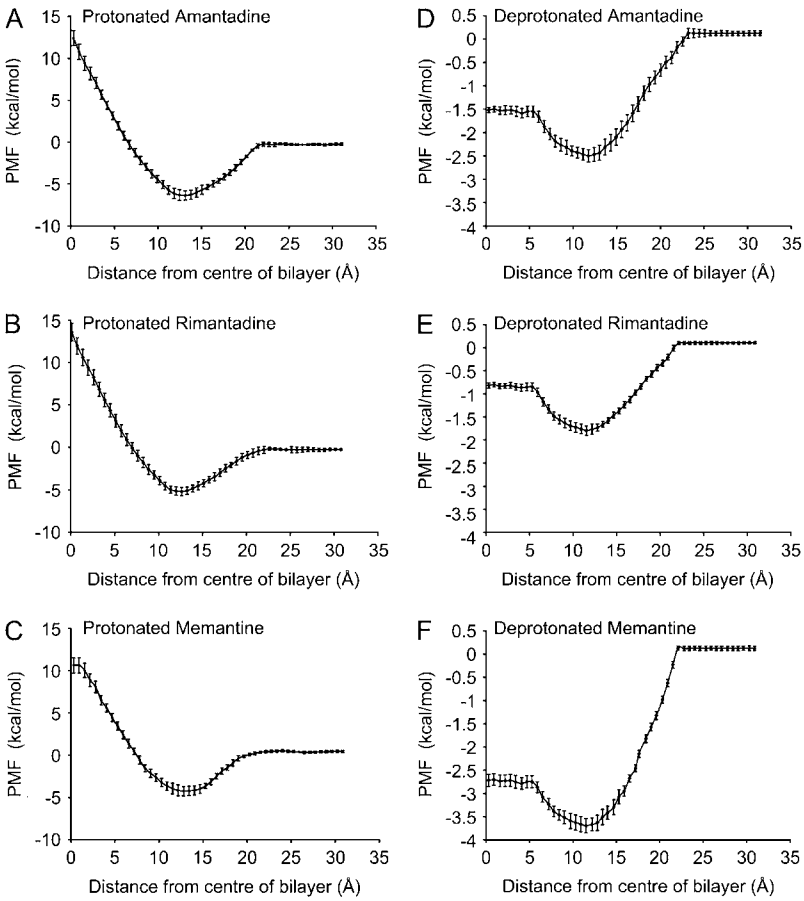

FIGURE 2 PMF for protonated amantadine (*A*), protonated rimantadine (*B*), protonated memantine (*C*), deprotonated amantadine (*D*), deprotonated rimantadine (*E*), and deprotonated memantine (*F*). Center of bilayer is located at 0. Error bars indicate standard error of the mean, derived from the block-averaging procedure described in text.

Interaction with the membrane

All three protonated forms of the adamantanes form substantial interactions with the lipid headgroups, even when located close to the bilayer center (Fig. 3). Consistent with previous reports on charged amino-acid side chains, the interactions between compounds and lipid headgroups lead to considerable deformation of the membrane, which also allows water molecules to form interactions with the ammonium moiety (Fig. 3). Such water interactions were previously observed in acetic acid in lipid bilayers (62), in valproic acid (82), and in the solvation of amino side-chains (69,70,83,84).

Based on the PMF (Fig. 2) and inspection of the trajectories, we can observe the mode of interaction of the adamantanes with the membrane. As they approach the headgroups of the POPC lipids (from $z = -40$ Å to -20 Å, and from $z = 40$ Å to 20 Å), they orient themselves such that the positive charge of the ammonium group faces the negatively charged phosphates (Fig. 3, *A*, *C*, and *E*). As a result, the PMFs start to decrease (Fig. 2). As they move closer to the interfacial region, the orientation of the adamantane flips 180° with respect to the bilayer (Fig. 3, *B*, *D*, and *F*), and it reaches an energy-minimum position in the PMF profile. Adamantanes remain in this orientation until they cross the center of the bilayer, where they flip such that the ammonium group orients to face the headgroups of the other lipid leaflet.

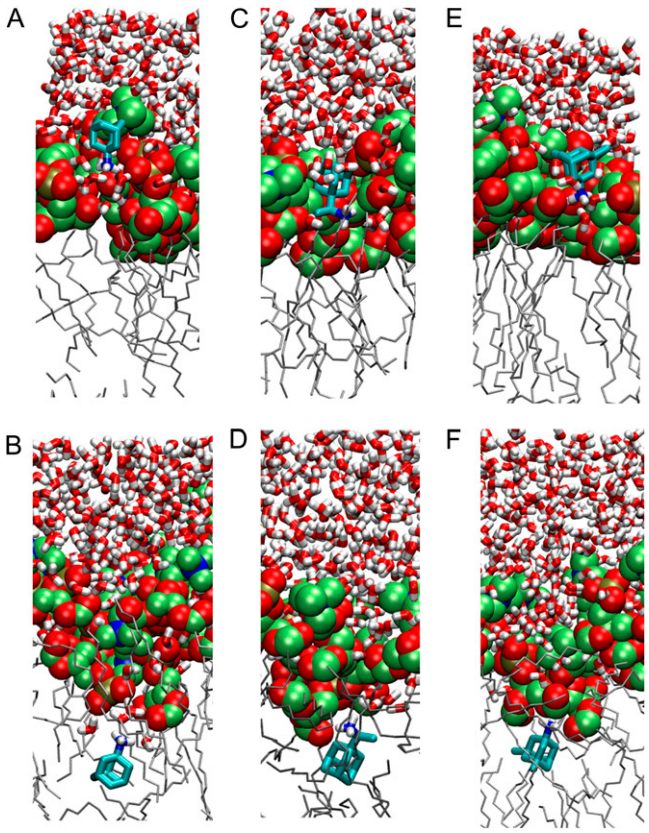

FIGURE 3 Preferred orientations near interface for amantadine (*A* and *B*), rimantadine (*C* and *D*) and memantine (*E* and *F*).

In the interface region where the PMF is at a minimum, the adamantanes appears to adopt a distinct orientation. To quantify this, we examined the orientation of the vector of the bond between the tricycle-decane group and the first atom of the substituent. Fig. 4 *A* shows the combined distribution (for amantadine) of windows between $z = 11$–14 Å and $z = -14$ to -11 Å. Similar distributions were obtained for rimantadine and memantine (data not shown). The distribution suggests an angle between 20–30°, consistent with recently reported solid-state NMR experiments (85). We also examined the radial distribution function (RDF) for the ammonium group of amantadine with various chemical moieties, as shown in Fig. 4, *B* and *C*. The RDFs show that for the interfacial location, the predominant interaction of the ammonium group is with the glycerol oxygens rather than those of the phosphate group. However, when amantadine is situated in the center of the bilayer, interactions with different oxygen groups are similar. Similar observations were made for rimantadine and memantine (data not shown).

We combined the PMF profiles of protonated and deprotonated forms to give the change in pK_a relative to the adamantanes in solution ($pK_{a;amantadine} = 9$ (86,87), $pK_{a;rimantadine} = 10.4$ (87), and $pK_{a;memantine} = 10.3$ (88,89), in accordance with the thermodynamic cycle shown in Fig. 5. The free energy for deprotonation in bulk water is calculated from the pK_a values, whereas the transfer free energies are computed directly from the PMFs. Thus, in a fashion similar to that of previous work (77,90), we can compute change in pK_a as a function of membrane depth with respect to bulk solution.

The results for amantadine (Fig. 6 *A*) indicate that the pK_a is reduced by 9 pH units in the center of the bilayer, favoring formation of the deprotonated state. The interface regions, on the other hand, have a positive shift of ~4 pH units, favoring the protonated state in this region. Large shifts in pK_a were also evident at the center of the membrane for rimantadine and memantine (Fig. 6, *B* and *C*). Similar scale shifts were reported for lysine (77,90) and methyl-guanidine (90), suggesting that our results are in both quantitative and qualitative agreement. For example, MacCallum et al. (70,77) showed that a lysine side chain would have a pK_a of 2 at the center of the bilayer, and a value of 12.5 in the region of the interface. The pK_a of lysine in aqueous solution is 10.8. Rimantadine differs from amantadine and memantine in that the latter exhibit positive increases in pK_a in the interface region, but rimantadine has no such change associated with it.

DISCUSSION

Implications for adamantanes as drugs

The PMF profiles suggest that the preferred location of adamantanes is in the interfacial region of the lipid bilayer, in agreement with recent experiments (41–43). The orientation is such that the tricyclo-decane moiety is in contact with the lipid alkyl chains, and the ammonium group is in

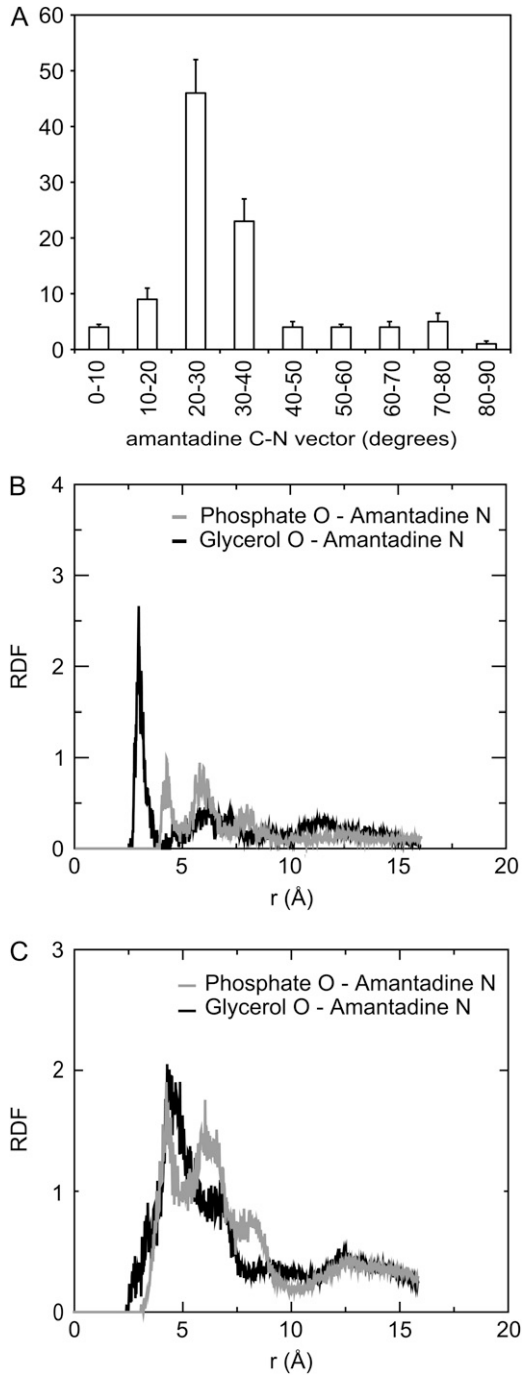

FIGURE 4 (*A*) Histogram of C-N vector-bilayer normal angle taken from simulation windows (both positive and negative with respect to center of bilayer) ± 11–14 Å of protonated amantadine. (*B*) Representative radial distribution function of oxygen atoms with respect to nitrogen atom of amantadine in the interface region ($z = -12$ Å). (*C*) Radial distribution function of oxygen atoms of phosphates and glycerol backbone with respect to nitrogen atom of amantadine in hydrophobic core of membrane ($z = 0$ Å).

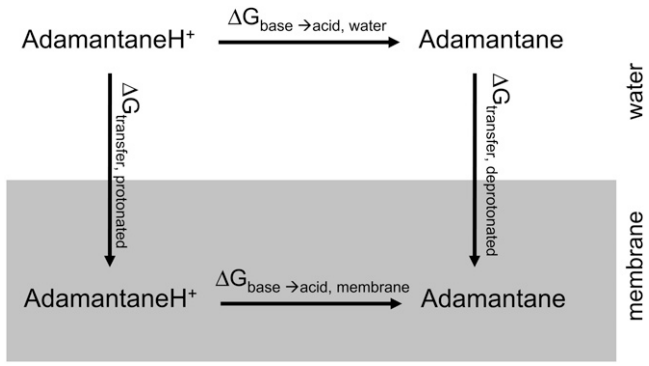

FIGURE 5 Thermodynamic cycle used to calculate change in pK_a value. Two transfer values are calculated directly from potentials of mean force for protonated and deprotonated forms of adamantanes. The $\Delta G_{\text{base} \rightarrow \text{acid, water}}$ is calculated directly from pK_a, as described in text.

contact with the lipid headgroups and in particular the glycerol oxygens. A recent NMR and MD study by Li et al. (85) also concluded that amantadine has a distinct population that resides in the interface region, and that the amine headgroup also interacts with the choline and glycerol oxygens.

Furthermore, this location is favorable with respect to bulk water, and thus raises questions about how these compounds interact with target proteins. For example, amantadine and rimantadine are known to interact with (and inhibit) the M2 channel from influenza A (1,3–5) and the p7 protein from HCV (6), whereas memantine is a known NMDA receptor block (22,24). Two structures for the M2 channel in complex with either amantadine (37) or rimantadine (38) were recently reported, but with differing proposed modes of action. Amantadine is thought to block the channel, whereas rimantadine is thought to interact on the exterior of the channel. Because there is no barrier for the absorption of amantadine or rimantadine to occupy an interfacial location (Fig. 2 *B*), these results support the idea that these compounds could first partition into the bilayer before interacting with its target protein (91,92). Moreover, several mutations of the M2 channel (93,94) that confer amantadine resistance to influenza A (at residue positions 26, 27, 30, 31, or 34) are located at a position in the bilayer that could be readily accessible from amantadine that has already absorbed to the interface as well as from the aqueous solution.

Although a recently determined structure supports the hypothesis that amantadine sits within the tetramer (33,34,95,96), it is still unclear how it would reach this site. If amantadine does need to sit inside the pore to effect a block, some movement of the M2 helices is likely. It is already known that the conformation of M2 helices depends on the lipid environment (97), suggesting a certain degree of plasticity in this region that might allow amantadine to enter from the lipid phase. It should also be remembered that both the x-ray and NMR structures are of truncated peptides, and it is not known to what extent the dynamics of the full-length protein differ from these shorter constructs.

The profiles of both the protonated and deprotonated forms of adamantanes allow for speculation about how these and other drugs might cross the lipid bilayer. Such information is

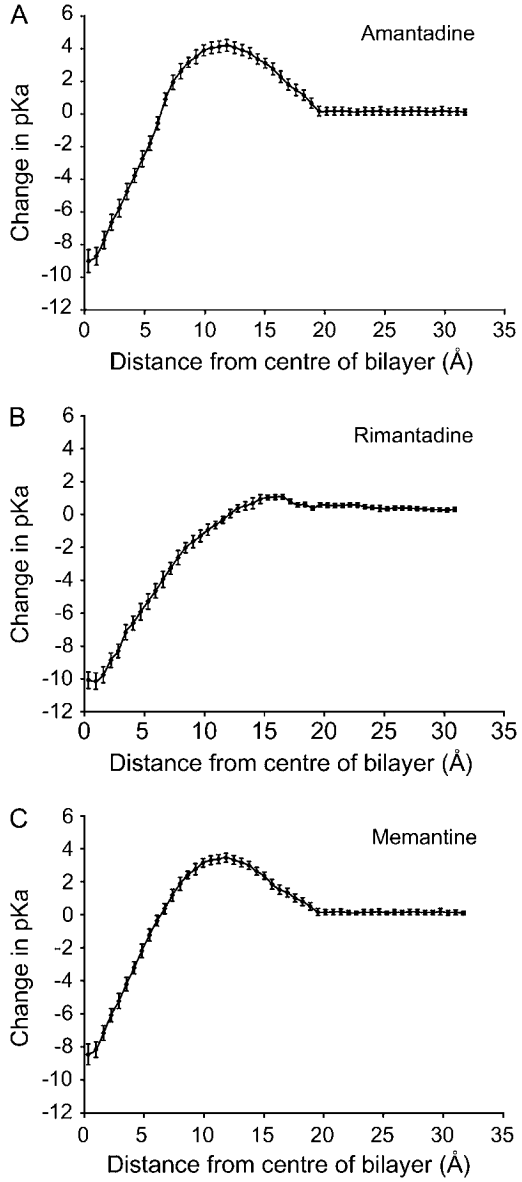

FIGURE 6 Change in pK_a (protonation of nitrogen) as a function of membrane depth for amantadine (*A*), rimantadine (*B*), and memantine (*C*). Error bars indicate standard error of the mean, according to the block-averaging procedure described in text.

particularly sought after, given that 98% of all new central nervous system candidate drugs do not cross the blood-brain barrier efficiently (98). There is no barrier to absorption to the interface region of the membrane, but there are differences in the size of the well, depending on the protonation state of the adamantane. For example, protonated amantadine has a well on the order of −6.5 kcal/mol, whereas for the deprotonated state, the well is only 2.5 kcal/mol. Similarly, protonated rimantadine has a well of −5.2 kcal/mol, whereas for the deprotonated state, the well is only 1.8 kcal/mol. Although there is also a difference for the protonated versus deprotonated state of memantine, the difference between them is somewhat smaller (−4.25 kcal/mol for the protonated state, versus −3.7 kcal/mol for the deprotonated state).

For all three compounds, the center of the bilayer presents a large barrier to permeation for the protonated species. The deprotonated species at this position, on the other hand, is slightly favorable compared with bulk (ranging from −0.8 kcal/mol for deprotonated rimantadine, to 2.7 kcal/mol for memantine). Thus one might expect the deprotonated species to be more likely the permeant species. The fraction of permeant species can be computed directly from the pK_a value. For example, with a pK_a of 9, amantadine will be 97.5% protonated (assuming a pH of 7.4 for the blood-brain barrier in vivo). Thus, 2.5% will be deprotonated. For this species to permeate, it must first absorb into the favorable well, hop over the central barrier (+ 1 kcal/mol with respect to the interface for deprotonated amantadine; Fig. 2 *D*) into the favorable energy well in the second lipid leaflet, where it must finally escape the second −2.5 kcal/mol energy well.

It is also of interest to compare the mode of interaction of these molecules and those of other small molecules with lipid bilayers. Simple alcohols are among the best-studied compounds in terms of their interactions with lipid bilayers (see Terama et al. (99) and references therein), with much of the work focusing on the effects of alcohol on the properties of the membrane. Patra et al. (100) analyzed the interactions of ethanol and methanol with lipid, and concluded that ethanol could interact with the ester groups of the lipids. Methanol was observed not to penetrate the lipid bilayer, and was presumably too polar overall. Dickey and Faller (101) observed that the OH group of propanol and butanol (at low concentrations) has greater interaction with the carbonyl groups of dipalmitoylphosphatidylcholine bilayers than ethanol, possibly reflecting an increase in van der Waals interactions between alkyl chains. Mukhopadhyay et al. examined the behavior and interaction of pentachlorophenol (PCP) with lipid bilayers (102). They found that the hydroxyl group interacted with the lipid carbonyl groups and water molecules, whereas PCP interacted with the alkyl chains in a parallel orientation, to optimize local packing in the dense ordered chain region of the bilayer. Thus, although the compounds reported in these studies and those reported here are quite dissimilar, they illustrate that the interfacial region of the lipid bilayer provides a suitable environment for a wide range of chemical groups, as long as they possess a large enough hydrophobic group (at least the size of ethanol) and a group capable of forming hydrogen bonds with the lipid carbonyl groups.

Limitations

It is important to note possible sources of error associated with this type of calculation: 1), System-size dependence: to investigate dependence on the size of a system, we repeated the calculation with two larger systems: one with 128 POPC lipids, and a second with 256 POPC lipids (see the Supple-

mentary Material, Data S1). In our simulations, we estimated the associated error to be up to 1 kcal mol^{-1}, in agreement with Allen et al. (103), who estimated an error of up to 1.8 kcal mol^{-1} that could be attributed to system size; 2), We used a nonpolarizable force field. Allen et al. (103) examined the influence of polarizability in detail, and concluded that a polarizable phospholipid could contribute a stabilizing effect of -3.6 ± 0.3 kcal mol^{-1}. More recently, Vorobyov et al. demonstrated that for an arginine analogue (the positively charged methyl guanidinium ion), the PMF computed with a Drude polarizable membrane reduced the barrier in the center of the bilayer by less than 1 kcal/mol, compared with PMFs calculated with the nonpolarizable CHARMM force-field (104). This was perhaps a smaller effect than might be expected (especially considering that the solvation free energy of a charged arginine in cyclohexane is substantially underestimated), but can be attributed to the shielding from the lipid hydrocarbon tails by water molecules and lipid headgroups because of the severe deformation of the membrane when a charged arginine is present. A similar level of membrane deformation was observed in the presence of charged species in this study, and thus we suggest that a similar level of error would likely be associated with these calculations; 3), Parameter choice: the interactions between lipids and these compounds were not explicitly validated. The underlying assumption is that previously derived parameters are transferable to similar systems. A similar assumption was made previously (77). To assess the influence of parameters on our results, we repeated the amantadine calculations with a different parameter set (Supplementary Material, Data S1). Those results gave remarkably similar profiles. Comparing the profiles for amantadine (Fig. 2, *A* and *D*) with the OPLS-AA force-field parameter set (Fig. S6, Data S1) shows that the error associated with the choice of parameter set is on the order of 0.5 kcal/mol.

CONCLUSIONS

We were able to demonstrate the preferred location of adamantane derivatives within a lipid bilayer. Furthermore, we showed that amantadine and rimantadine are likely to be protonated at this interfacial location in POPC lipids. Memantine, on the other hand, has only a slight preference for the protonated state at this position. These aspects are likely to be important for an understanding of how these compounds reach their targets within the cell.

Our results also suggest that the membrane-permeant species in all cases is likely to be the deprotonated form. Whether that deprotonation step proceeds in the bulk solution or after initial absorption into the interface region remains to be seen.

The complexity of profiles highlights the dangers of trying to compare membrane affinity with drug permeability (60,105), and demonstrates that the membrane cannot be treated as a simple continuum slab. A similar conclusion was reached through recent work on charged amino-acid side chains in membranes (106). Such considerations will be important for a better understanding of drug designs.

SUPPLEMENTARY MATERIAL

To view all of the supplemental files associated with this article, visit www.biophysj.org.

We thank our colleagues for useful discussions, and in particular, Ranjit Vijayan, Mark Sansom, Chze Ling Wee, and Nicole Zitzmann.

We thank the Wellcome Trust for support. C.F.C. thanks the Overseas Research Scheme for support, and the National Grid Service for computer time. P.C.B. is a Research Councils of United Kingdom Fellow.

REFERENCES

1. Pinto, L. H., and R. A. Lamb. 2007. Controlling influenza virus replication by inhibiting its proton channel. *Mol. Biosyst.* 3:18–23.
2. Blanchet, P. J., L. V. Metman, and T. N. Chase. 2003. Renaissance of amantadine in the treatment of Parkinson's disease. *Adv. Neurol.* 91:251–257.
3. Davies, W. L., R. R. Grunert, R. F. Haff, J. W. McGahen, E. M. Neumayer, M. Paulshock, J. C. Watts, T. R. Wood, E. C. Herrman, and C. E. Hoffman. 1964. Antiviral activity of 1-adamantadine (amantadine). *Science.* 144:862–863.
4. Hay, A. J., A. J. Wolstenholme, J. J. Skehel, and M. H. Smith. 1985. The molecular basis of the specific anti-influenza action of amantadine. *EMBO J.* 4:3021–3024.
5. Pinto, L. H., L. J. Holsinger, and R. A. Lamb. 1992. Influenza virus M_2 protein has ion channel activity. *Cell.* 69:517–528.
6. Griffin, S. D., L. P. Beales, D. S. Clarke, O. Worsfold, S. D. Evans, J. Jaeger, M. P. Harris, and D. J. Rowlands. 2003. The p7 protein of hepatitis C virus forms an ion channel that is blocked by the antiviral drug, amantadine. *FEBS Lett.* 535:34–38.
7. Steinmann, E., T. Whitfield, S. Kallis, R. A. Dwek, N. Zitzmann, T. Pietschmann, and R. Bartenschlager. 2007. Antiviral effects of amantadine and iminosugar derivatives against hepatitis C virus. *Hepatology.* 46:330–338.
8. Riley, T. R., and M. R. Taheri. 2007. Long-term treatment with the combination of amantadine and ribavirin in hepatitis C nonresponders. A case series. *Dig. Dis. Sci.* 52:3418–3422.
9. Brillanti, S., F. Levantesi, L. Masi, M. Foli, and L. Bolondi. 2000. Triple antiviral therapy as a new option for patients with interferon nonresponsive chronic hepatitis C. *Hepatology.* 32:630–634.
10. Deltenre, P., J. Henrion, V. Canva, S. Dharancy, F. Texier, A. Louvet, S. De Maeght, J. C. Paris, and P. Mathurin. 2004. Evaluation of amantadine in chronic hepatitis C: a meta-analysis. *J. Hepatol.* 41:462–473.
11. Mangia, A., G. Leandro, B. Helbling, E. L. Renner, M. Tabone, L. Sidoli, S. Caronia, G. R. Foster, S. Zeuzem, T. Berg, V. Di Marco, N. Cino, and A. Andriulli. 2004. Combination therapy with amantadine and interferon in naive patients with chronic hepatitis C: meta-analysis of individual patient data from six clinical trials. *J. Hepatol.* 40:478–483.
12. Mangia, A., G. L. Ricci, M. Persico, N. Minerva, V. Carretta, D. Bacca, M. Cela, M. Piattelli, M. Annese, G. Maio, D. Conte, V. Guadagnino, V. Pazienza, D. Festi, F. Spirito, and A. Andriulli. 2005. A randomized controlled trial of pegylated interferon alpha-2a (40KD) or interferon alpha-2a plus ribavirin and amantadine vs interferon alpha-2a and ribavirin in treatment-naive patients with chronic hepatitis C. *J. Viral Hepat.* 12:292–299.
13. Berg, T., B. Kronenberger, H. Hinrichsen, T. Gerlach, P. Buggisch, E. Herrmann, U. Spengler, T. Goeser, S. Nasser, K. Wursthorn, G. R. Pape, U. Hopf, and S. Zeuzem. 2003. Triple therapy with amantadine

in treatment-naive patients with chronic hepatitis C: a placebo-controlled trial. *Hepatology.* 37:1359–1367.

14. Ciancio, A., A. Picciotto, C. Giordanino, A. Smedile, M. Tabone, A. Manca, G. Marenco, P. Garbagnoli, M. Andreoni, G. Cariti, G. Calleri, M. Sartori, S. Cusumano, A. Grasso, R. Rizzi, M. Gallo, M. Basso, M. Anselmo, G. Percario, G. Ciccone, M. Rizzetto, and G. Saracco. 2006. A randomized trial of pegylated-interferon-alpha2a plus ribavirin with or without amantadine in the re-treatment of patients with chronic hepatitis C not responding to standard interferon and ribavirin. *Aliment. Pharmacol. Ther.* 24:1079–1086.
15. Craxi, A., and O. Lo Lacono. 2001. Amantadine for chronic hepatitis C: a magic bullet or yet another dead duck? *J. Hepatol.* 35:527–530.
16. Khalili, M., C. Denham, and R. Perrillo. 2000. Interferon and ribavirin versus interferon and amantadine in interferon nonresponders with chronic hepatitis C. *Am. J. Gastroenterol.* 95:1284–1289.
17. Thuluvath, P. J., A. Maheshwari, J. Mehdi, K. D. Fairbanks, L. L. Wu, L. G. Gelrud, M. J. Ryan, F. A. Anania, I. F. Lobis, and M. Black. 2004. Randomised, double blind, placebo controlled trial of interferon, ribavirin, and amantadine versus interferon, ribavirin, and placebo in treatment naive patients with chronic hepatitis C. *Gut.* 53:130–135.
18. Kilpatrick, G. J., and G. S. Tilbrook. 2002. Memantine. Merz. *Curr. Opin. Investig. Drugs.* 3:798–806.
19. Oxford, J. S., and A. Galbraith. 1980. Antiviral activity of amantadine: a review of laboratory and clinical data. *Pharmacol. Ther.* 11:181–262.
20. Jackish, R., T. Link, B. Neufang, and R. Koch. 1992. Studies on the mechanism of action of the antiparkinsonian drugs memantine and amantadine: no evidence for direct dopaminergic or antimuscurinic properties. *Arch. Int. Pharmacodyn. Ther.* 320:21–42.
21. Danielczyk, W. 1995. Twenty-five years of amantadine therapy in Parkinson's disease. *J. Neural Transm. Suppl.* 46:399–405.
22. Alisky, J. M. 2007. Successful treatment of Parkinson's disease with memantine. *South. Med. J.* 100:617.
23. Eldefrawi, A. T., E. R. Miller, D. L. Murphy, and M. E. Eldefrawi. 1982. [3H] Phencyclidine interactions with the nicotinic acetylcholine receptor channel and its inhibition by psychotropic, antipsychotic, opiate, antidepressant, antibiotic, antiviral and antiarrhythmic drugs. *Mol. Pharm.* 22:72–81.
24. Lipton, S. A. 2006. Paradigm shift in neuroprotection by NMDA receptor blockade: memantine and beyond. *Nat. Rev. Drug Discov.* 5:160–170.
25. Jensen, A. A., B. Frølund, T. Liljefors, and P. Krogsgaard-Larsen. 2005. Neuronal nicotinic acetylcholine receptors: structural revelations, target identifications and therapeutic inspirations. *J. Med. Chem.* 48:4705–4745.
26. Francis, P. T. 2008. Glutamatergic approaches to the treatment of cognitive and behavioural symptoms of Alzheimer's disease. *Neurodegener. Dis.* 5:241–243.
27. Cheung, W., L. Guo, and M. F. Cordeiro. 2008. Neuroprotection in glaucoma: drug-based approaches. *Optom. Vis. Sci.* 85:406–416.
28. Freisleben, H. J., G. Waltinger, W. Schatton, and G. Zimmer. 1989. Influences of tromantadine and nonoxinol 9 on the stability of red cell membrane. Arzneim. Forsch. Drug Res. 39:1202–1205.
29. Phonphok, Y., and K. S. Rosenthal. 1991. Stabilization of clathrin coated vesicles by amantadine, tromantadine and other hydrophobic amines. *FEBS Lett.* 281:188–190.
30. Jain, M. K., N. Yen-Min Wu, T. K. Morgan, M. S. Briggs, and R. K. J. Murray. 1976. Phase transition in a lipid bilayer. II. Influence of amantadine derivatives. *Chem. Phys. Lipids.* 17:71–78.
31. Sansom, M. S. P., and I. D. Kerr. 1993. Influenza virus M2 protein: a molecular modelling study of the ion channel. *Protein Eng.* 6:65–74.
32. Pinto, L. H., and R. A. Lamb. 1995. Understanding the mechanism of action of the anti-influenza virus drug amantadine. *Trends Microbiol.* 3:271.
33. Astrahan, P., I. Kass, M. A. Cooper, and I. T. Arkin. 2004. A novel method of resistance for influenza against a channel-blocking antiviral drug. *Proteins.* 55:251–257.
34. Hu, J., T. Asbury, S. Achuthan, C. Li, R. Bertram, J. R. Quine, R. Fu, and T. A. Cross. 2007. Backbone structure of the amantadine-blocked trans-membrane domain M2 proton channel from influenza A virus. *Biophys. J.* 92:4335–4343.
35. Salom, D., B. R. Hill, J. D. Lear, and W. F. DeGrado. 2000. pH-Dependent tetramerization and amantadine binding of the transmembrane helix of M2 from the influenza A virus. *Biochemistry.* 39:14160–14170.
36. Wang, C., K. Takeuchi, L. H. Pinto, and R. A. Lamb. 1993. Ion channel activity of influenza A virus M_2 protein: characterization of the amantadine block. *J. Virol.* 67:5585–5594.
37. Stouffer, A. L., R. Acharya, D. Salom, A. S. Levine, L. Di Costanzo, C. S. Soto, V. Tereshko, V. Nanda, S. Stayrook, and W. F. DeGrado. 2008. Structural basis for the function and inhibition of an influenza virus proton channel. *Nature.* 451:596–599.
38. Schnell, J. R., and J. J. Chou. 2008. Structure and mechanism of the M2 proton channel of influenza A virus. *Nature.* 451:591–595.
39. Cady, S. D., and M. Hong. 2008. Amantadine-induced conformational and dynamical changes of the influenza M2 transmembrane proton channel. *Proc. Natl. Acad. Sci. USA.* 105:1483–1488.
40. Balaz, S. 2000. Lipophilicity in trans-bilayer transport and subcellular pharmacokinetics. *Perspect. Drug Discov. Des.* 19:157–177.
41. Duff, K. C., P. J. Gilchrist, A. M. Saxena, and J. P. Bradshaw. 1994. Neutron diffraction reveals the site of amantadine blockade of the influenza A M2 ion channels. *Virology.* 202:287–293.
42. Wang, J., J. R. Schnell, and J. J. Chou. 2004. Amantadine partition and localization in phospholipid membrane: a solution NMR study. *Biochem. Biophys. Res. Commun.* 324:212–217.
43. Subczynski, W. K., J. Wojas, V. Pezeshk, and A. Pezeshk. 1998. Partitioning and localization of spin-labeled amantadine in lipid bilayers: an EPR study. *J. Pharm. Sci.* 87:1249–1254.
44. Skehel, J. J. 1992. Influenza virus. Amantadine blocks the channel. *Nature.* 358:110–111.
45. Bright, R. A., M.-J. Medina, X. Xu, G. Perez-Oronoz, T. R. Wallis, X. M. Davis, L. Povinelli, N. J. Cox, and A. I. Klimov. 2005. Incidence of adamantane resistance among influenza A (H3N2) viruses isolated worldwide from 1994–2005: a cause for concern. *Lancet.* 366:1175–1181.
46. Deyde, V. M., X. Xu, R. A. Bright, M. Shaw, C. B. Smith, Y. Zhang, Y. Shu, L. V. Gubareva, N. J. Cox, and A. I. Klimov. 2007. Surveillance of resistance to adamantanes among influenza A (H3N2) and A (H1N1) viruses isolated worldwide. *J. Infect. Dis.* 196:249–257.
47. de Clercq, E., and J. Neyts. 2007. Avian influenza A (H5N1) infection: targets and strategies for chemotherapeutic intervention. *Trends Pharmacol. Sci.* 28:280–285.
48. Bright, R. A., D. K. Shay, B. Shu, N. J. Cox, and A. I. Klimov. 2006. Adamantane resistance among influenza A viruses isolated early during the 2005–2006 influenza season in the United States. *JAMA.* 295:891–894.
49. Barr, I. G., A. C. Hurt, N. Deed, P. Ianello, C. Tomasov, and N. Komadina. 2007. The emergence of adamantane resistance in influenza A (H1) viruses in Australia and regionally in 2006. *Antiviral Res.* 75:173–176.
50. Saito, R., D. Li, and H. Suzuki. 2007. Amantadine-resistant influenza A (H3N2) virus in Japan, 2005–2006. *N. Engl. J. Med.* 356:312–313.
51. Pohorille, A., M. H. New, K. Schweighofer, and M. A. Wilson. 1999. Insights from computer simulations into the interaction of small molecules with lipid bilayers. *Curr. Top. Membr. Trans.* 48:49–76.
52. Bassolino-Klimas, D., H. E. Alper, and T. R. Stouch. 1993. Solute diffusion in lipid bilayer membranes: an atomic level study by molecular dynamics simulation. *Biochemistry.* 32:12624–12637.

53. Bassolino-Klimas, D., H. E. Alper, and T. R. Stouch. 1995. Mechanism of solute diffusion through lipid bilayer membranes by molecular dynamics simulation. *J. Am. Chem. Soc.* 117:4118–4129.
54. Alper, H. E., and T. R. Stouch. 1995. Orientation and diffusion of a drug analog in biomembranes—molecular dynamics simulations. *J. Phys. Chem.* 99:5724–5731.
55. Stouch, T. R., H. E. Alper, and D. Bassolino. 1995. Simulations of drug diffusion in biomembranes. *ACS Symp. Ser.* 589:127–138.
56. Cascales, L. J. J., H. J. G. Cifre, and G. J. de laTorre. 1998. Anaesthetic mechanism on a model biological membrane: a molecular dynamics simulation study. *J. Phys. Chem. B.* 102:625–631.
57. Koubi, L., M. Tarek, S. Bandyopadhyay, M. L. Klein, and D. Scharf. 2001. Membrane structural perturbations caused by anesthetics and nonimmobilizers: a molecular dynamics investigation. *Biophys. J.* 81:3339–3345.
58. Vemparala, S., L. Saiz, R. G. Eckenhoff, and M. L. Klein. 2006. Partitioning of anesthetics into a lipid bilayer and their interaction with membrane-bound peptide bundles. *Biophys. J.* 91:2815–2825.
59. Högberg, C. J., A. Maliniak, and A. P. Lyubartsev. 2007. Dynamical and structural properties of charged and uncharged lidocaine in a lipid bilayer. *Biophys. Chem.* 125:416–424.
60. Bemporad, D., C. Luttmann, and J. W. Essex. 2004. Computer simulation of small molecule permeation across a lipid bilayer: dependence on bilayer properties and solute volume, size and cross-sectional area. *Biophys. J.* 87:1–13.
61. Bemporad, D., J. W. Essex, and C. Luttmann. 2004. Permeation of small molecules through a lipid bilayer: a computer simulation study. *J. Phys. Chem. B.* 108:4875–4884.
62. Bemporad, D., C. Luttmann, and J. W. Essex. 2005. Behaviour of small solutes and large drugs in a lipid bilayer from computer simulations. *Biochim. Biophys. Acta.* 1718:1–21.
63. King, P. M. 1993. Free energy via molecular simulation: a primer. *In* Computer Simulation of Biomolecular Systems. W. F. Van Gunsteren, P. K. Weiner, and A. J. Wilkinson, editors. ESCOM, Leiden. 267–314.
64. Torrie, G. M., and J. P. Valleau. 1977. Nonphysical sampling distributions in Monte Carlo free-energy estimation: umbrella sampling. *J. Comput. Phys.* 23:187–199.
65. Allen, T. W., O. S. Andersen, and B. Roux. 2006. Molecular dynamics—potential of mean force calculations as a tool for understanding ion permeation and selectivity in narrow channels. *Biophys. Chem.* 124:251–267.
66. Beckstein, O., and M. S. P. Sansom. 2006. A hydrophobic gate in an ion channel: the closed state of the nicotinic acetylcholine receptor. *Phys. Biol.* 3:147–159.
67. Tieleman, D. P., and S.-J. Marrink. 2006. Lipids out of equilibrium: energetics of desorption and pore mediated flip-flop. *J. Am. Chem. Soc.* 128:12462–12467.
68. Norman, K. E., and H. Nymeyer. 2006. Indole localization in lipid membranes revealed by molecular simulation. *Biophys. J.* 91:2046–2054.
69. Dorairaj, S., and T. W. Allen. 2007. On the thermodynamic stability of a charged arginine side chain in a transmembrane helix. *Proc. Natl. Acad. Sci. USA.* 104:4943–4948.
70. MacCallum, J. L., W. F. Bennett, and D. P. Tieleman. 2007. Partitioning of amino acid side chains into lipid bilayers: results from computer simulations and comparison to experiment. *J. Gen. Physiol.* 129:6206–6210.
71. Hermans, J., H. J. C. Berendsen, W. F. van Gunsteren, and J. P. M. Postma. 1984. A consistent empirical potential for water-protein interactions. *Biopolymers.* 23:1513–1518.
72. Schuettelkopf, A. W., and D. M. F. van Aalten. 2004. PRODRG—a tool for high-throughput crystallography of protein-ligand complexes. *Acta Crystallogr. D Biol. Crystallogr.* 60:1355–1363.
73. Schiferl, S. K., and D. C. Wallace. 1985. Statistical errors in molecular dynamics averages. *J. Chem. Phys.* 83:5203–5209.
74. van der Spoel, D., E. Lindahl, B. Hess, G. Groenhof, A. E. Mark, and H. J. C. Berendsen. 2005. GROMACS: fast, flexible and free. *J. Comput. Chem.* 26:1701–1718.
75. Jorgensen, W. L., D. S. Maxwell, and J. Tirado-Rives. 1996. Development and testing of the OPLS all-atom force field on conformational energetics and properties of organic liquids. *J. Am. Chem. Soc.* 118:11225–11236.
76. Coll, E. P., C. Kandt, D. A. Bird, A. L. Samuels, and D. P. Tieleman. 2007. The distribution and conformation of very long-chain plant wax components in a lipid bilayer. *J. Phys. Chem. B.* 111:8702–8704.
77. MacCallum, J. L., W. F. D. Bennett, and D. P. Tieleman. 2008. Distribution of amino acids in a lipid bilayer from computer simulations. *Biophys. J.* 94:3393–3404.
78. Berendsen, H. J. C., J. P. M. Postma, W. F. van Gunsteren, A. DiNola, and J. R. Haak. 1984. Molecular dynamics with coupling to an external bath. *J. Chem. Phys.* 81:3684–3690.
79. Berger, O., O. Edholm, and F. Jahnig. 1997. Molecular dynamics simulations of a fluid bilayer of dipalmitoylphosphatidycholine at full hydration, constant pressure and constant temperature. *Biophys. J.* 72:2002–2013.
80. Darden, T., D. York, and L. Pedersen. 1993. Particle mesh Ewald—an N.log(N) method for Ewald sums in large systems. *J. Chem. Phys.* 98:10089–10092.
81. Humphrey, W., A. Dalke, and K. Schulten. 1996. VMD—visual molecular dynamics. *J. Mol. Graph.* 14:33–38.
82. Ulander, J., and A. D. J. Haymet. 2003. Permeation across hydrated dppc lipid bilayers: simulation of the titrable amphophilic drug valproic acid. *Biophys. J.* 85:3475–3484.
83. Freites, J. A., D. J. Tobias, G. von Heijne, and S. H. White. 2005. Interface connections of a transmembrane voltage sensor. *Proc. Natl. Acad. Sci. USA.* 102:15059–15064.
84. Johansson, A. C., and E. Lindahl. 2006. Amino-acid solvation structure in transmembrane helices from molecular dynamics simulations. *Biophys. J.* 91:4450–4463.
85. Li, C., M. Yi, J. Hu, H.-X. Zhou, and T. A. Cross. 2008. Solid-state NMR and MD simulations of the antiviral drug amantadine solubilized in DMPC bilayers. *Biophys. J.* 94:1295–1302.
86. Bleidner, W. E., J. B. Harmon, W. E. Hewes, T. E. Lynes, and E. C. Hermann. 1965. Absorption, distribution and excretion of amantadine hydrochloride. *J. Pharmacol. Exp. Ther.* 150:484–490.
87. Spector, R. 1988. Transport of amantadine and rimantadine through the blood-brain barrier. *J. Pharmacol. Exp. Ther.* 244:516–519.
88. Wesemann, W., K. H. Sontag, and J. Maj. 1983. Pharmacodynamics and pharmacokinetics of memantine. Arzneim. Forsch. Drug Res. 33:1122–1134.
89. Freudenthaler, S., I. Meineke, F. H. Schreeb, E. Boakye, U. Gundert-Remy, and C. H. Gleiter. 1998. Influence of urine pH and urinary flow on the renal excretion of memantine. *Br. J. Clin. Pharmacol.* 46:541–546.
90. Li, L., I. Vorobyov, A. D. MacKerell Jr., and T. W. Allen. 2008. Is arginine charged in a membrane? *Biophys. J.* 94:L11–L13.
91. Mason, R. P., D. G. Rhodes, and L. G. Herbette. 1991. Reevaluating equilibrium and kinetic binding parameters for lipophilic drugs based on a structural model for drug interaction with biological membranes. *J. Med. Chem.* 34:869–877.
92. Kolocouris, A., R. K. Hansen, and R. W. Broadhurst. 2004. Interaction between an amantadine analogue and the transmembrane portion of the influenza A M2 protein in liposomes probed by ^{1}H NMR spectroscopy of the ligand. *J. Med. Chem.* 47:4975–4978.
93. Hay, A. J., M. C. Zambon, A. J. Wolstenholme, J. J. Skehel, and M. H. Smith. 1986. Molecular basis of resistance of influenza A viruses to amantadine. *J. Antimicrob. Chemother.* 8(Suppl. B):19–29.
94. Belshe, R. B., M. H. Smith, C. B. Hall, R. Betts, and A. J. Hay. 1988. Genetic basis of resistance to rimantadine emerging during treatment of influenza virus infection. *J. Virol.* 62:1508–1512.
95. Reference deleted in proof.

96. Stouffer, A. L., V. Nanda, J. D. Lear, and W. F. DeGrado. 2005. Sequence determinants of a transmembrane proton channel: an inverse relationship between stability and function. *J. Mol. Biol.* 347:169–179.

97. Duong-Ly, K. C., V. Nanda, W. F. DeGrado, and K. P. Howard. 2005. The conformation of the pore region of the M2 proton channel depends on the lipid bilayer environment. *Protein Sci.* 14:856–861.

98. Terasaki, T., and W. M. Pardridge. 2000. Targeted drug delivery to the brain (blood-brain barrier, efflux, endothelium, biological transport). *J. Drug Target.* 8:353–355.

99. Terama, E., O. H. S. Ollila, E. Salonen, A. C. Rowat, C. Trandum, P. Westh, M. Patra, M. Karttunen, and I. Vattulainen. 2008. Influence of ethanol on lipid membranes: from lateral pressure profiles to dynamics and partitioning. *J. Phys. Chem. B.* 112:4131–4139.

100. Patra, M., E. Salonen, E. Terama, I. Vattulainen, R. Faller, B. W. Lee, J. Holopainen, and M. Karttunen. 2006. Under the influence of alcohol: the effect of ethanol and methanol on lipid bilayers. *Biophys. J.* 90:1121–1135.

101. Dickey, A. N., and R. Faller. 2007. How alcohol chain-length and concentration modulate hydrogen bond formation in a lipid bilayer. *Biophys. J.* 92:2366–2376.

102. Mukhopadhyay, P., H. J. Vogel, and D. P. Tieleman. 2004. Distribution of pentachlorophenol in phospholipid bilayers: a molecular dynamics study. *Biophys. J.* 86:337–345.

103. Allen, T. W., O. S. Andersen, and B. Roux. 2006. Ion permeation through a narrow channel: using gramicidin to ascertain all-atom molecular dynamics potential of mean force methodology and biomolecular force-fields. *Biophys. J.* 90:3447–3468.

104. Vorobyov, I., L. Li, and T. W. Allen. 2008. Assessing atomistic and coarse-grained force fields for protein-lipid interactions: the formidable challenge of an ionizable side chain in a membrane. *J. Phys. Chem. B.* 112:9588–9602.

105. Thomae, A. V., T. Koch, C. Panse, H. Wunderli-Allenspach, and S. D. Krämer. 2007. Comparing the lipid membrane affinity and permeation of drug-like acids: the intriguing effects of cholesterol and charged lipids. *Pharm. Res.* 24:1457–1472.

106. Allen, T. W. 2007. Modeling charged side-chains in lipid membranes. *J. Gen. Physiol.* 130:237–240.